LIMNOLOGY and OCEANOGRAPHY

ASLO

Limnol. Oceanogr. 66, 2021, 3116–3133

doi: 10.1002/lno.11864

Rapid changes in river plume dynamics caused by advected wind-driven coastal upwelling as observed in Lake Geneva

Frédéric Soulignac,[1*,a] **Ulrich Lemmin**,[1] **Seyed Mahmood Hamze Ziabari**,[1] **Htet Kyi Wynn**,[1] **Benjamin Graf**,[1] **David Andrew Barry**[1]

[1]Ecological Engineering Laboratory (ECOL), Institute of Environmental Engineering (IIE), Faculty of Architecture, Civil and Environmental Engineering (ENAC), Ecole Polytechnique Fédérale de Lausanne (EPFL), Lausanne, Switzerland

Abstract

Based on field investigations carried out in Lake Geneva during summer stratification in 2019, this study documents, for the first time, the rapid change of negatively buoyant river inflow dynamics caused by the passing of a coastal upwelling. Under calm conditions, the negatively buoyant Rhône River, entering at the eastern end of the lake, interacts with the lake density profile such that the river intrusion moves as an interflow in the thermocline layer straight out into the lake. A strong, large-scale spatially homogeneous wind that lasts for several days causes a downward thermocline tilt at the western end of the lake, coastal downwelling on the northern shore, and coastal upwelling on the southern shore. This cold-water upwelling progresses like a Kelvin wave around the lake after wind forcing ceases. When it arrives at the river inflow area, it homogenizes the lake water temperatures, and the river inflow transforms into an intrusion that spreads over the whole water column. Trapped by strong alongshore currents generated by the progressing coastal upwelling, the river plume is sharply deviated and flows along the shore in the nearshore zone, potentially bringing nutrients directly into the phototrophic near-surface layer. Following the passage of the coastal upwelling, the river inflow transforms back into an interflow. This change in inflow dynamics, which is documented for five strong wind events between June and September by combining in situ measurements, remote sensing, and numerical simulation, can be expected to occur in other large lakes with comparable wind-induced large-scale thermocline displacement.

Introduction

Lakes are water bodies of great ecological and societal value. They often serve as drinking water reservoirs, and support fishery and recreational activities, such as bathing and boating, all of which require good water quality. Rivers play an important role in maintaining or deteriorating lake water quality. For example, rivers can discharge pollutants and nutrients that potentially contribute to harmful phytoplankton development in lakes (Allan et al. 1983; Zhao et al. 2013). On the other hand, restoration of lake water quality can be achieved by artificially feeding clean rivers into poor water quality lakes (Welch 1981; Shinohara et al. 2008). It is therefore important to determine the pathways taken by rivers in lakes and the associated water mixing in order to understand lake ecosystem functioning and to develop effective water management policies. Rivers enter lakes in the near shore zone; and in large lakes, large-scale processes occurring in this zone, such as coastal upwelling and downwelling and Kelvin waves, can affect their pathway. In the present study carried out in Lake Geneva, we document for the first time how two large-scale processes, that is, a negatively buoyant river inflow and a counterclockwise progressing coastal upwelling interact with each other and cause a rapid change in the river pathway.

The pathways followed by river intrusions in lakes are the result of the interplay between river properties (discharge and density), the lake density profile in the vicinity of the river mouth, and the background currents in the lake. River intrusions can take two different forms: (1) if the river density is lower than or equal to that of the lake surface layer, the discharge is found within that layer (Jirka 2007), or (2) negatively buoyant inflows displace lake surface waters up to the plunge point where the river intrusion abruptly sinks and follows the lakebed as an underflow (Alavian et al. 1992). Depending on the lake density profile, after plunging, the underflow

*Correspondence: frederic.soulignac@epfl.ch, f.soulignac@cipel.org

Additional Supporting Information may be found in the online version of this article.

[a]Present address: Commission internationale pour la protection des eaux du Léman (CIPEL), Nyon, Switzerland

detaches from the lakebed at the depth where river and lake densities are comparable, and transforms into an interflow. This conceptual framework has been applied to describe negatively buoyant river inflows in stratified lakes (Giovanoli and Lambert 1985; Churchill et al. 2003; Hogg et al. 2013; Scheu et al. 2015) where river interflows develop in a layer at the base of the lake surface mixed layer just above the abrupt change of water density in the thermocline.

In the near shore zone of large lakes, wind-driven coastal upwelling is an important transport process that occurs due to offshore Ekman transport. It brings deep cold and dense water masses towards the upper layer of the nearshore zone by displacing the thermocline upwards, thus replacing the warmer water in that layer (Plattner et al. 2006; Oesch et al. 2008; Reiss et al. 2020). During "full" upwelling, the thermocline reaches the lake surface (Csanady 1977). Coastal upwelling generates strong alongshore currents in the nearshore zone (Reiss et al. 2020). A key feature of coastal upwelling is that, after strong wind events cease, the region of coastal upwelling progresses counterclockwise around the lake basin as a thermal front at a speed comparable to that of an internal Kelvin wave (Mortimer 1974, 1988; Csanady 1977; Simons and Schertzer 1987). Some indications of this upwelling progression were also detected on lake surfaces by remote sensing (Csanady 1977; Mortimer 1988; Bolgrien and Brooks 1992). Numerical modeling confirms the counterclockwise Kelvin wave-like progression of cold coastal upwelling fronts as the upwelling relaxes after a wind event (Beletsky et al. 1997). The modeling results provided full upwelling and subsequent progressing relaxation patterns that are qualitatively similar to the above observations. Thus, coastal upwelling events progressing counterclockwise around the lake basin successively expose near shore zones along their path temporarily to destratification and high alongshore currents, even though no wind forcing actually occurred in those zones. As will be shown in the present study for Lake Geneva, the pathway dynamics of rivers entering lakes, in particular for small rivers whose dynamics are not controlled by Coriolis forcing, are strongly affected by the passage of this counterclockwise progressing coastal upwelling.

In the marine environment and in estuaries, the interaction of a buoyant river inflow with coastal upwelling events was examined previously (Gan et al. 2009; Osadchiev et al. 2020). For a buoyant river plume in Lake Ontario, Masse and Murthy (1990) found that coastal downwelling events concentrate the plume into a coastal current. Model results suggest that, in Lake Erie, the offshore supply of phosphorus via upwelling and river input is of ecological significance for the near-shore zone (Valipour et al. 2016). Other studies focused on the impact of coastal upwelling events on river outflow conditions, in particular, thermal regimes (Laval et al. 2008; Lisi and Schindler 2015).

However, the interaction of the two independent phenomena, that is, a negatively buoyant river inflow and a counterclockwise progressing coastal upwelling event, is not documented in the literature, even though, as will be demonstrated in this study, it is a commonly occurring transient process. During the passage of a counterclockwise progressing cold-water coastal upwelling front, the near shore zone stratification in front of the river mouth is temporarily changed, and thus the plunge dynamics of the river is modified. A negatively buoyant river plume now finds its equilibrium depth either much closer to the lake surface, or at the lake surface in the case of full upwelling. At the same time, the river plume is entrained into the strong counterclockwise-oriented alongshore currents. The transient interaction of the river plume with the changing stratification and current speeds has the potential of affecting, albeit only temporarily, the ecosystem dynamics in adjacent areas of the near shore zone of a lake. However, due to the frequent recurrence of this sequence of processes, the cumulative effect over time may be significant.

The objective of the present study is to make evident in detail, and for the first time, the interaction of a counterclockwise progressing coastal upwelling event and a negatively buoyant river plume in a large lake (Lake Geneva) during the stratification period. The following questions will be addressed:

- How do lake stratification and currents change in the nearshore zone during the passage of a counterclockwise progressing coastal upwelling?
- What effect does this have on the structure of the river inflow?
- How is the path of the river inflow altered by the passage of the counterclockwise progressing coastal upwelling?
- Can this have an impact on water quality?
- How do these newly documented findings affect current concepts of negatively buoyant river inflows entering stratified lakes?

The inflow of the Rhône River into Lake Geneva is an ideal study site for this investigation because background data are all known with good spatial and temporal resolution from publicly available sources. In the present study, these data were supplemented by a detailed field investigation in the Rhône River delta area. Furthermore, three-dimensional (3D) whole-lake numerical simulations were carried out and revealed that counterclockwise progressing coastal upwelling is the large-scale process that can explain the observed interaction between river inflow and the flow field in the lake.

A Supporting Information section provides details and clarifications of aspects discussed in the text.

Materials and methods

Study site

Lake Geneva (also called *Lac Léman*) is a large, deep monomictic lake located at the border between France and Switzerland. It is the largest freshwater lake in Western Europe with a length of ~70 km, a maximum width of 14 km, a volume of

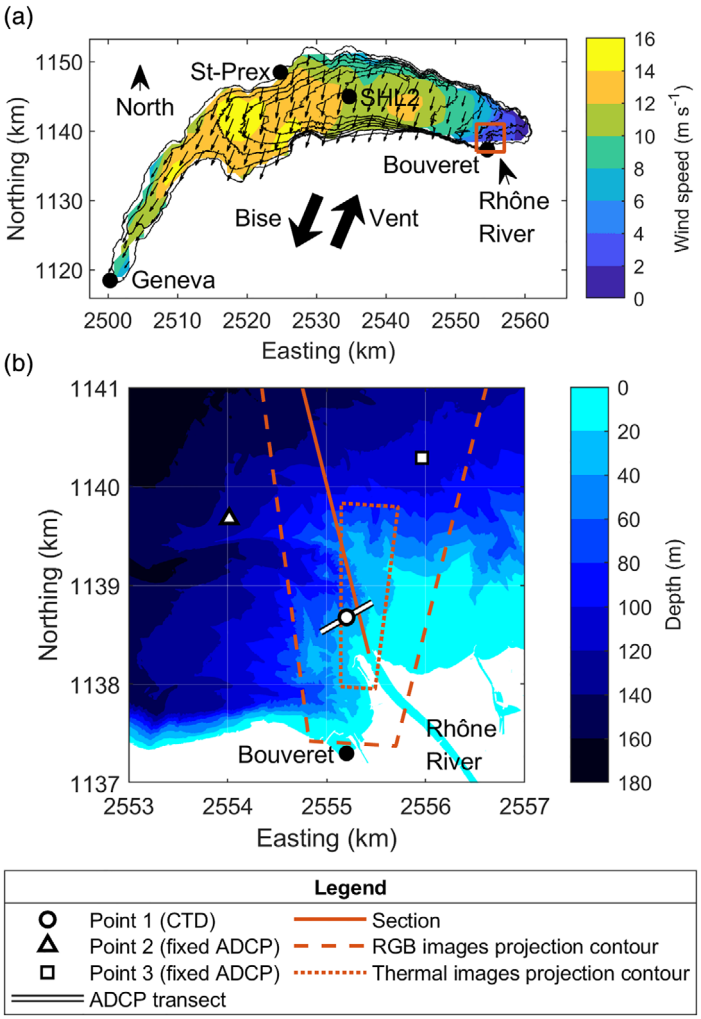

Fig. 1. (**a**) Map of Lake Geneva showing depth contours (50, 100,150, 200, 250, and 300 m) and mean wind speed (color bar) and direction (small black arrows) for a *Bise* wind event on 16 July 2019 (COSMO data). The directions of the two strong dominant winds called *Bise* and *Vent* are indicated with large arrows. CIPEL monitoring station SHL2 is situated in the deepest part of Lake Geneva (309 m); limnigraphs are installed at St.-Prex and Geneva; and the red square delimits the Bouveret area (*see* zoom in Fig. 1b). The Swiss coordinate system (CH1903+) is used (Swiss Federal Office of Topography, http://www.swisstopo.admin.ch). (**b**) Zoom of the Bouveret area (red square in Fig. 1a) where the Rhône River, the lake's main inflow, enters the lake. Measurement points and camera viewing areas are listed in the legend. "Section" refers to Fig. 6a results; for details *see* text.

90 km^3, a surface area of 582 km^2, and a maximum depth of 309 m (Fig. 1a). The lake is composed of two basins: the small, narrow shallow basin (maximum depth 75 m) called *Petit Lac* to the west, and the large deep (maximum depth 309 m) *Grand Lac* to the east. Lake Geneva thermally stratifies in summer, and its surface temperature frequently reaches 25°C by late summer with a thermocline situated at approximately 15-m depth. The temperature in the deep hypolimnion layers never exceeds 6°C. Due to its large size, Coriolis force effects have been shown to be important in the momentum balance of the lake (Lemmin et al. 2005; Cimatoribus et al. 2018; Lemmin 2020). The inertial period at the latitude of Lake Geneva is approximately 16.5 h (Bauer et al. 1981).

The wind field over the lake is guided by the surrounding mountainous topography and dominated by two strong winds: the *Vent* from the southwest and the *Bise* from the northeast (Graf and Prost 1980; Wanner and Furger 1990; Lemmin and D'Adamo 1996). These winds blow over most of the lake surface. Strong wind events are largely responsible for the energy transfer from the atmosphere into the lake and strongly impact the currents of Lake Geneva (Lemmin and D'Adamo 1996; Lemmin et al. 2005). The Bouveret area, where the Rhône River enters Lake Geneva, is sheltered during *Bise* events due to the surrounding high mountains (Fig. 1a).

Rhône River

The Rhône River is the principal source of water and sediments for Lake Geneva. It enters the lake at the eastern end of the lake near Bouveret (Fig. 1a). From 1965 to 2018, it provided on average 73% of the water discharged annually at the outflow at the western end of the lake basin at Geneva (mean discharge 245.6 m^3 s^{-1}). The mean annual discharge shows long-term stability, with yearly fluctuations related to precipitation intensity and snow accumulation. In summer, the river temperature ranges between 8°C and 11°C.

During the study period (24 June to 15 September 2019), the average values of river temperature and conductivity were 9.81°C (SD 0.81°C) and 201.3 μS cm^{-1} (SD 33.5 μS cm^{-1}). The base level of suspended sediment concentration in the river was approximately 200 mg l^{-1}, and the concentration reached high values during high discharge events (maximum 4705 mg l^{-1} on 3 July). For the five events, the average daily flow discharge, temperature, and suspended sediment concentration of the Rhône River are summarized in Table ST1. Profiles taken every 2 weeks at the monitoring station SHL2 (*see* Fig. 1a for location), located at the deepest point (309 m) of the lake, indicate that the surface temperature in the top 5 m varied between 19°C and 27.6°C, that is, it was always higher than the river temperature. The conductivity difference between the river and the lake is very small, and the suspended sediment concentration in the central part of the lake is assumed to be negligible and thus not measured.

The importance of Earth rotation on the Rhône River plume can be estimated by the Kelvin number (Krauss 1973; Churchill et al. 2003; Demchenko et al. 2017), $K = b/ri$, where b is the river width and ri is the internal Rossby deformation radius, ($ri = [g' h]^{1/2}/f$), with g' the reduced gravity, h the mean depth of the river, and f the local Coriolis parameter. When K is small ($K \ll 1$), the dynamics of the plume can be treated as nonrotating ($f = 0$). Using the values indicated above, a river width of 120 m and a mean depth of 5 m, we obtain a K ranging from 0.02 to 0.05. Thus, the Rhône River can be considered a small river (Garvine 1995) and Coriolis force does

not affect its plume. However, the dynamics of the Rhône River plume can be controlled by the large-scale motion field in the lake. The flushing time of Lake Geneva (also referred to as theoretical residence time in the literature; Monsen et al. 2002) of approximately 11 yr (CIPEL 2019) further confirms that river throughflow is small and has a limited effect on the large-scale motion field in the lake.

From the onset of lake thermal stratification and due to the density difference between the river and the lake surface, the river forms an interflow under calm conditions that detaches from the lakebed, as described in the Introduction (Dominik et al. 1983; Giovanoli and Lambert 1985; Giovanoli 1990). During occasional high discharge events when the Rhône River carries a high sediment charge, the river inflow breaks through the thermocline and flows as a turbidity current through a subaquatic canyon, carrying sediments mainly as bedload, down into the deep hypolimnion (Loizeau and Dominik 2000; Kremer et al. 2015; Corella et al. 2016).

Available data

Meteorological data for the Alpine region with a grid box size of 1.1 km and an hourly time-step are provided by the Consortium for Small-scale Modeling (COSMO, http://www.cosmo-model.org). The data include the required parameters to perform 3D hydrodynamic simulations of lakes, that is, wind speed and direction, air temperature, relative humidity of air, atmospheric pressure, incident solar radiation, and cloud cover. These data are made available by MeteoSwiss (https://www.meteoswiss.admin.ch). COSMO wind data are presented in Fig. 1a for a typical *Bise* event. COSMO model outputs are systematically verified by MeteoSwiss against in situ measurements from synoptic and automatic stations located in Switzerland and Europe. We used the assimilated outputs (called analysis data), based on observational data from all of Switzerland, rather than forecast data (Voudouri et al. 2017). The validity of these data was evaluated in a comparison with data from meteorological field stations around the lake (Rahaghi et al. 2018).

In the present study, *Bise* wind events that occurred during the period when moored ADCP measurements were taken in the Rhône River delta (24 June to 15 September 2019) were investigated. They were selected based on COSMO wind data according to the following criteria: (1) average daily wind speed was greater than 5 ms^{-1} for at least two consecutive days and (2) highest wind speed was greater than 10 ms^{-1}. Five episodes of 5 d were found that each contained a single *Bise* event. Wind speeds for the five episodes are summarized in Table ST1. The wind pattern was different for each episode (Fig. S1). The strongest *Bise* event occurred during Episode 2 when detailed field measurements were made in the Rhône River delta. This episode is presented in detail below, and similar results for the other four episodes are given in the Supporting Information (Appendix S1).

The Lake Geneva water level is monitored by limnigraphs at Geneva and St.-Prex by the Swiss Federal Office for the Environment (FOEN, https://www.bafu.admin.ch); the locations of the monitoring stations are shown in Fig. 1a. FOEN also provides Rhône River data. At Porte de Scex, situated 5 km upstream of the river mouth, the river stage, temperature, and conductivity are recorded with a 5-min time step. Suspended sediment concentrations are manually recorded approximately twice a week.

Long-term monitoring of Lake Geneva temperature is performed by profile measurements taken at station SHL2 (*see* Fig. 1a) by the Alpine Center for Research on Trophic Networks and Limnic Ecosystems (CARRTEL, https://www6.lyon-grenoble.inrae.fr/carrtel) of the French National Research Institute for Agriculture, Food and Environment (INRAE, https://www.inrae.fr), and the International Commission for the Protection of Lake Geneva Waters (CIPEL, https://www.cipel.org). In summer, this monitoring is carried out twice a month (© OLA-IS, AnaEE-France, INRAE of Thonon-les-Bains, CIPEL; Rimet et al. 2020).

Field instrumentation

The sets of instrumentation that were employed for the present study are summarized in Table 1. To monitor the surface signature of the river inflow, RGB and thermal time-lapse cameras were installed 3 km south of the river inflow on a mountain overlooking Bouveret, at approximately 740 m above the lake. RGB images were analyzed with Matlab software using the functions created by Emmanuel Farhi (https://github.com/farhi/matlab-readraw, last accessed 27 April 2020). RGB and thermal images were projected onto the lake surface, assimilated to a horizontal surface, and geo-referenced (*see* Fig. 1b for the location of the projection contours of the RGB and thermal images). The resulting resolution in the Bouveret area of interest is of the order of 1 m $pixel^{-1}$.

Current profiles, spaced 0.7–1.4 m horizontally, were measured using an Acoustic Doppler Current Profiler (ADCP) mounted on a boat-towed catamaran. Near-surface and near bottom currents were omitted in all ADCP measurements because of transient signals from the pulse transmission that saturate the system's electronics and because of acoustic reflections. The tilt and heading angles were derived from a sensor located inside the instrument and were used to correct the data. ADCP velocities with a low echo amplitude signal (<70 counts) were removed. A moving average over 180 s was applied for both components (East–West and North–South) together with a moving average in the vertical direction over 3 m thick layers.

Three-dimensional hydrodynamic simulation

The 3D hydrodynamic model MITgcm was originally designed to capture large-scale/global to small-scale/regional processes in oceans (Marshall et al. 1997). It has also been successfully applied to lakes (Dorostkar et al. 2017). The

capability of the model to realistically reproduce the stratification, mean flow, internal seiche variability, and upwelling in Lake Geneva was assessed and confirmed by Cimatoribus et al. (2018, 2019) and Reiss et al. (2020) after careful calibration of the model. The model integrates the 3D Reynolds-averaged Navier–Stokes equations on a sphere under the Boussinesq and both the hydrostatic and nonhydrostatic approximations (Marshall et al. 1997). The hydrostatic mode of the model with an implicit free surface was used in this study. The horizontal subgrid-scale mixing can be defined with either a constant eddy viscosity or nonlinear Smagorinsky viscosities. Here, Smagorinsky molecular (Laplacian) horizontal viscosity with a coefficient of 0.3 and biharmonic viscosity with a coefficient A4 = 0.01 were applied (Griffies and Hallberg 2000). The vertical subgrid-scale mixing of scalars is defined using the turbulent closure scheme K-profile parameterization of Large et al. (1994). The surface is forced by realistic atmospheric fields from COSMO data (Voudouri et al. 2017) as described earlier. The model uses the bulk formulation from Large and Pond (1981) to compute the atmospheric fluxes. Following Cimatoribus et al. (2018), we first initialized our modeling in 2018 with a Low-Resolution (LR) version of the model, and then initialized a High-Resolution (HR) version in 2019 with the output of the LR version for that date and ran it for the study period (July to September 2019). The initial dates of both the HR and LR models were chosen based on calm wind conditions for several days, thus allowing the model to have enough time to adjust to the initial conditions.

Model bathymetry was interpolated from the high resolution (2 m × 2 m) survey conducted by the Canton Vaud (Switzerland) in 2014 (https://www.asitvd.ch, last accessed 17 January 2018). The LR grid had a horizontal resolution of 173–260 m and 35 depth layers in the vertical direction. It was initialized from rest on 2 July 2018, using the temperature profile available at SHL2 on that date as a horizontally uniform initial temperature condition. The integration time step of the LR grid model was set 20 s and a 6-month spin up was carried out. The HR model was initialized using the results of the LR model on 17 April 2019, and integrated over an 8-month period. The horizontal resolution of the HR model was 113 m with 50 depth layers. The vertical Z-level spacing was 0.35 m at the surface, which gradually increased to a maximum of 12 m at the deepest part of the lake. The HR initial time step was set to 6 s for numerical stability.

Results

Lake Geneva hydrodynamics excited by Bise wind events

The lake water level measured at Geneva and the COSMO wind data show that *Bise* events push the lake surface water towards Geneva and thus raise the lake surface level by a few centimeters at the Geneva (western) end of the lake. This is clearly observable for Episode 2 (Fig. 2a), and for Episodes 3, 4, and 5 (Fig. S1). The five *Bise* events lasted longer than the inertial period of 16.5 h and generated a geostrophic adjustment. Due to Ekman transport, this adjustment raised the water level on the northern (Swiss) shore of the lake and lowered it on the southern (French) shore. The limnigraph of St.-Prex on the northern shore shows a buildup of water for Episode 2 (Fig. 2a). For the remaining episodes, lake level changes are presented in Fig. S1.

The numerical simulation indicates a thermocline downward tilt in the *Petit Lac* at Geneva for the five episodes (Fig. 2b for Episode 2; Fig. S2 for the remaining episodes). The thermocline that is initially positioned between 10 and 20-m depth, depending on the episode, is lowered during the *Bise* events down to almost 40-m depth for Episode 2. The numerical simulation also shows a coastal downwelling of the thermocline on the Swiss northern shore (Fig. 2c), and a coastal upwelling of cold water along the French southern shore up to the Bouveret area (Fig. 2d for Episode 2; Fig. S2 for the remaining episodes).

For Episode 2, the simulation predicts that the thermocline almost reaches the surface in the coastal upwelling area. After the *Bise* wind ceased, the coastal upwelling/downwelling pattern exhibits a Kelvin wave-like counterclockwise rotation around the lake basin (Fig. 3). The coastal upwelling, which arrives at the Bouveret area in the morning of 16 July, brings cold water masses with a temperature of around 10°C in the 2.5-m thick model layer at 11.3–13.8-m depth. This layer is representative of the thermocline at rest. Twelve hours later, the upwelling has left the Bouveret area and continues toward the north, following the Swiss shore (Fig. 3). A similar pattern of counterclockwise rotation of the coastal upwelling is predicted by the numerical simulation for the remaining episodes (Fig. S3).

Time series of the modeled temperatures at Points 2 and 3 confirm the change in temperature during the passage of the upwelling in front of the Rhône River inflow (Fig. 4a). Temperatures near the surface only dip slightly. However, in a 20-m deep layer below, stratification is progressively being eroded, while the coastal upwelling advances and temperatures decrease to those measured in the Rhône River. Temperatures then again begin to rise and stratification is re-established after the upwelling has left the Bouveret area. The predicted vertical displacement of the thermocline is validated by the CTD profiles taken on 16 and 17 July 2019 in the Rhône delta area when the coastal upwelling passed through the Bouveret area (Fig. 4b). On 16 July at Point 1, the vertical temperature profile shows that the thermocline was in the near surface layer. On 17 July 2019, after the upwelling has left the Bouveret area (Fig. 3), the surface mixed layer extends down to 15 m at the same monitoring station; this is the typical thermocline depth for that time of the year. Modeled and measured temperatures agree well as can also be seen in the temperature development during the time interval between the dashed vertical lines in Fig. 2d. Images taken by the time-

Table 1. Summary of field instrumentation. For station locations, *see* Fig. 1.

Measurement type	Instrument	Setting	Location	Period
Time-lapse camera	Nikon D3300 RGB camera with telephoto lens, Flir Tau2 540 infrared camera	RGB 24M pixels, infrared 0.2 M pixels, one image per min	3 km south of the river inflow on a mountain	Permanently recording
CTD profiles	Sea & Sun Marine Tech CTD 75M with turbidity sensor	42 samples per meter	Point 1 (*see* Fig. 1)	Transects on 16 and 17 July 2019
Towed ADCP	Teledyne RDI Workhorse Sentinel 300 kHz with bottom tracking	Mode 12; downward looking; bin size 1 m, 100 bins, sampling interval 1–2 s	Catamaran towed at 0.7 m s^{-1} along ADCP transect (*see* Fig. 1)	Transects on 16 and 17 July 2019
Moored ADCP	Teledyne RDI Workhorse Sentinel 300 kHz	Moored at 50 m depth; upward looking; bin size 1 m, sampling interval 10 min	Points 2 and 3 (*see* Fig. 1)	24 June to 15 September 2019

lapse camera on 16 July further suggest that cold-water upwelling almost reached the surface in the Bouveret area at that time, as documented by boat tracks (Fig. S4). Only during the passage of the coastal upwelling event does the water in the boat track have the same temperature as that in the Rhône River, indicating a thermocline near the lake surface.

Furthermore, the numerical simulation shows that the passage of the upwelling is accompanied by a current pattern in the near surface layer that travels in the nearshore zone around the lake basin. In the Bouveret area, this is confirmed by eastward near surface currents measured at Points 2 and 3 (Fig. 5 for Episode 2; Fig. S5 for the remaining episodes). The onset of this current, its duration, and the velocity amplitude are well captured by the numerical simulation. The mean absolute error between simulated and measured currents based on hourly data from 13 July 2019 to 18 July 2019 is 5.6 cm s^{-1}; this is approximately half of typical background lake currents. Despite the different wind patterns of the five *Bise* events, this current always occurs in the Bouveret area 40–50 h after each event (Fig. S5), which is close to half a Kelvin wave period in Lake Geneva (Lemmin et al. 2005).

The offshore extent of the currents related to the upwelling and the depth profile of the currents cannot be determined by the measurements. Instead, this information was obtained from numerical modeling. In Fig. 6a, the alongshore current component in a section extending from the river mouth out into the open lake is plotted for several instances during the passage of the coastal upwelling (*see* Fig. 1b for section location). Initially, when the cold-water coastal upwelling caused a homogenization of the lake water temperature (Fig. 4), currents are still weak (Fig. 5). Current speeds then progressively increased over time in a layer that extends outward from the shore. However, high currents are limited to a nearshore zone slightly extending past the locations of Points 2 and 3, and current speeds rapidly taper off with distance from shore beyond this layer. Further offshore, current speeds are in the range of typical values observed in the lake. Thus, the alongshore current pattern that follows the passage of the coastal upwelling is organized in a narrow, nearshore band. The depth of this band is restricted to the upper layer. This pattern can also be seen in the sequence of model results for the Bouveret area, depth-averaged over the upper layer (Fig. 6b). Figure 6b again shows that the current speeds rapidly taper off with distance from the shore. Stratification in the nearshore zone changes during the passage of the coastal upwelling, as can be seen from the modeled isotherms (Fig. 6a). In order to determine the potential of a small-scale interaction of the two water masses, gradient Richardson numbers were calculated from the modeled velocity and temperature field for the instances during the passage of the coastal upwelling shown in Fig. 6a. When the coastal upwelling reaches its maximum speed early on 17 July (Fig. 5), Richardson numbers fall to low values due to strong shear and weak stratification in the upper layer, indicating that mixing is likely (Fig. S16).

Rhône River plume dynamics

The impact of the sequence of processes taking place during the passage of the counterclockwise progressing coastal upwelling, that is, (1) a thermocline downward tilt in the *Petit Lac* at Geneva (Fig. 2), (2) the generation of cold-water coastal upwelling on the southern shore of the *Grand Lac* (Fig. 3), and (3) the passage of the strong eastward current in the near surface layer in the Bouveret area (Figs. 5 and 6) on the dynamics of the Rhône River plume is presented in detail for Episode 2. The overall effects of this sequence of processes for the other episodes are similar and shown in the Supporting Information (Figs. S6–S13).

On 16 July 2019, the RGB and thermal images taken by the time-lapse cameras between 11:00 and 16:00 indicate turbid and cold Rhône River water that does not sink (Figs. 7 and 8) and does not form a plunge point, as would be expected for

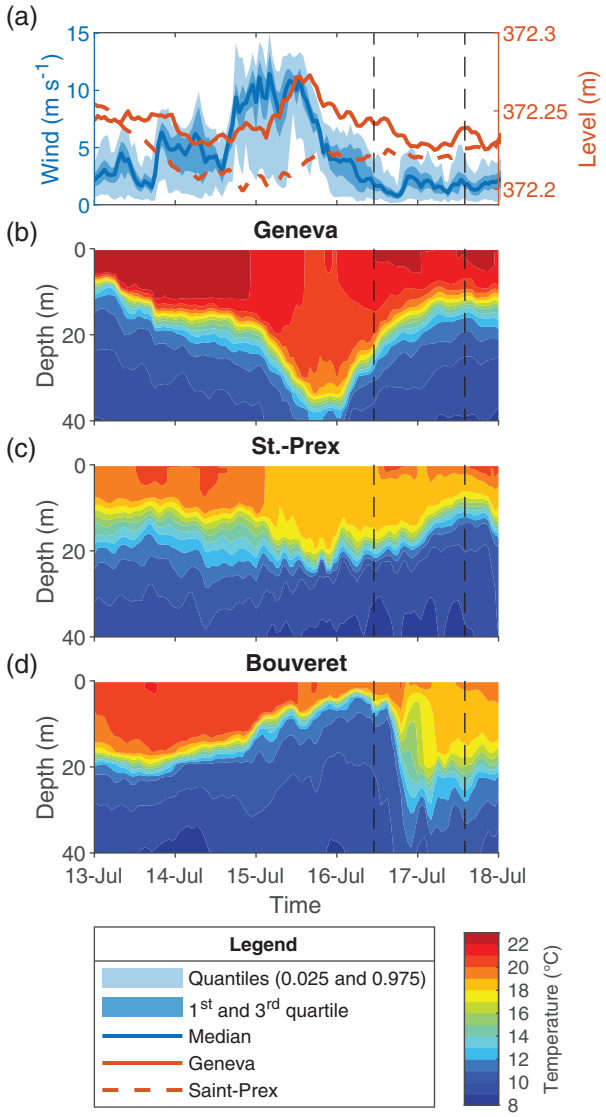

Fig. 2. (**a**) Time series of wind speed averaged over the lake surface (COSMO data, left y-axis, blue) and lake level (right *y*-axis, red) for Episode 2, and time series of vertical profiles of simulated temperature in the upper layers of Lake Geneva for Episode 2 at: (**b**) Geneva (*Petit Lac*), (**c**) St.-Prex (*Grand Lac*), and (**d**) Bouveret (*Grand Lac*). *See* Fig. 1a for locations. The transect field measurements in the Rhône Delta (near Bouveret) were taken during the period between the dashed vertical lines. Colors and lines are defined in the legend.

river discharge that is a negatively buoyant with respect to the ambient lake water. Instead, the river plume remains at the lake surface and spreads out up to several hundred meters from the river mouth.

Temperature profiles taken at Points 1 and 2 were comparable (Fig. 4b). These measurements and the simulation results (Fig. 4a) show that on 16 July, the thermocline had moved almost up to the surface, and that the temperature in the water column was nearly homogeneous and similar to the Rhône River temperature (*see* also Table ST1). Transparency and conductivity were likewise homogeneous over the whole water column, but were lower at Point 1 in front of the Rhône River inflow, than at Point 2 further to the west, which can be considered as a reference point for the ambient lake conditions. From Fig. 3, it is apparent that the cold-water coastal upwelling passes through the Bouveret area during that time.

The vertical profiles of current velocity measured on that date along the ADCP transect indicate that when there is no significant vertical density gradient in the lake, the river intrusion covers a volume that spans the whole water column from the lake surface to the bed, and over a 100-m width that is comparable to the Rhône River channel width (Fig. 9a). High current velocities corresponding to the river intrusion were measured over the whole water column in that volume, with higher values and a core zone more likely in the upper layer, suggesting that most of the inflow was in the upper layer, as also seen in the RGB and thermal images.

From the RGB images and in particular, the thermal images between 16 July at 17:00 and 17 July at 2:00 (Figs. 7 and 8), the river plume is suddenly (at 18:00) strongly and persistently deviated towards the east in the same direction as the counterclockwise progressing coastal upwelling. Velocities measured at Points 2 and 3, as well as those predicted by the numerical model (Figs. 5 and 6), have the highest eastward values during that time. They peak at around 0.5 m s^{-1}, which is much higher than typical background lake currents in this area (<0.1 m s^{-1}).

When the counterclockwise progressing coastal upwelling left the Bouveret area after midnight on 16 July (Fig. 4), the RGB and thermal images show that the eastward displacement of the river plume first gradually decreased and then, from 7:00 July 17 onward, it plunged shortly after the inflow, with the plunge line describing a quasi-isosceles triangle, the base of which coincides with the river mouth (Figs. 7 and 8). This is the plume surface pattern typical of negatively buoyant river plume interflow. The characteristic summer thermal stratification with a well-developed thermocline was re-established on 17 July at 10:00 in front of the river inflow (Fig. 4). In the transparency profiles at Point 1, a low transparency layer corresponding to an interflow of the turbid Rhône River plume is evident in the thermocline layer combined with a slightly lower conductivity, typical for the Rhône River in the same layer (Fig. 4b). The vertical profiles of current velocity measured along the ADCP transect on 17 July 2019 show that the river intrusion again detached from the lakebed at the depth of the thermocline layer as an interflow centered at around 20-m depth in the transect (Fig. 9a).

Since the upwelling progresses counterclockwise in the nearshore zone, its passage in the Bouveret area is accompanied by a strong eastward current in the upper layer in front of the river mouth (Figs. 5 and 6). This peak in the moored ADCP current recordings was measured at Points 2 and 3 approximately 45 h after the peak of the *Bise* event (Fig. S14). A well-developed eastward current was also seen in the upper layer in the ADCP profiles all along the transect on

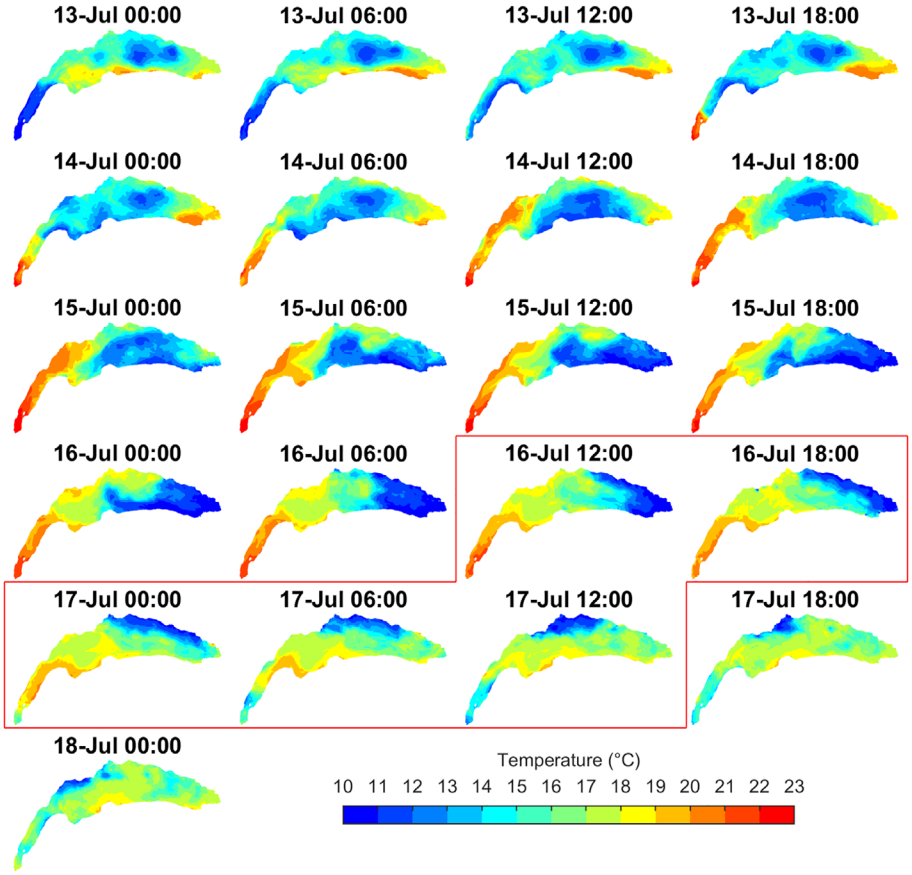

Fig. 3. Filled contour plots of simulated water temperature for Lake Geneva every 6 h in the 2.5-m thick model layer at 11.3–13.8-m depth for Episode 2. The transect field measurements in the Rhône delta (near Bouveret) were taken during the period delimited in red. The temperature range is given in the color bar.

17 July at 10:36 (Fig. 9a), indicating that the river water was transported to the east in the nearshore area. In agreement with the measured currents at Points 2 and 3 (Fig. 5) and those predicted by numerical modeling (Fig. 6a), it gradually decreased as the day went on. For Episode 2, the peak current velocities at the lake surface and at the river mouth had a similar magnitude (~0.3 m s^{-1}).

The pattern of the ADCP backscatter measured along the transect on those 2 days (Fig. 9b) confirms the above observations. On 16 July, when the currents were distributed over the whole water column, high backscattering was also detected in the whole water column. On 17 July, the Rhône River plume again formed an interflow and, as a consequence, no backscatter is evident in the upper layer of the water column. The maximum of the backscatter in the interflow layer agrees with the maximum in the current pattern (Fig. 9a).

For Episode 2, the sequence of processes described above, which took place during the passage of the cold-water coastal upwelling, is summarized in Fig. 10. A similar pattern in the structure of strong eastward alongshore currents at Points 2 and 3 following the passage of the coastal upwelling in the Bouveret area is evident in the remaining episodes (Fig. S5). Furthermore, the RGB and thermal images show an eastward deviation of the river plume in the nearshore zone in each of these episodes (Figs. S6–S13), suggesting that each *Bise*-induced coastal upwelling generates similar response patterns of the Rhône River plume in the Bouveret area, as described in detail for Episode 2 above.

Discussion

Coastal upwelling

The numerical simulation showed that the *Bise* event caused a thermocline downward tilt of about 20 m at the western (Geneva) end of the lake basin (Fig. 2b). A comparable tilt of the thermocline after a strong *Bise* event was previously observed from temperature profiles taken along the lake axis between the center of the lake near SHL2 (*see* Fig. 1a for station location; thermocline at about 20-m depth) and near Geneva (thermocline depth about 40 m) (Lemmin and D'Adamo 1996). The upwelling/downwelling pattern will turn into a Kelvin wave if no further strong wind event occurs. Following an event, up to four consecutive passages of Kelvin waves have been observed in Lake Geneva (Lemmin

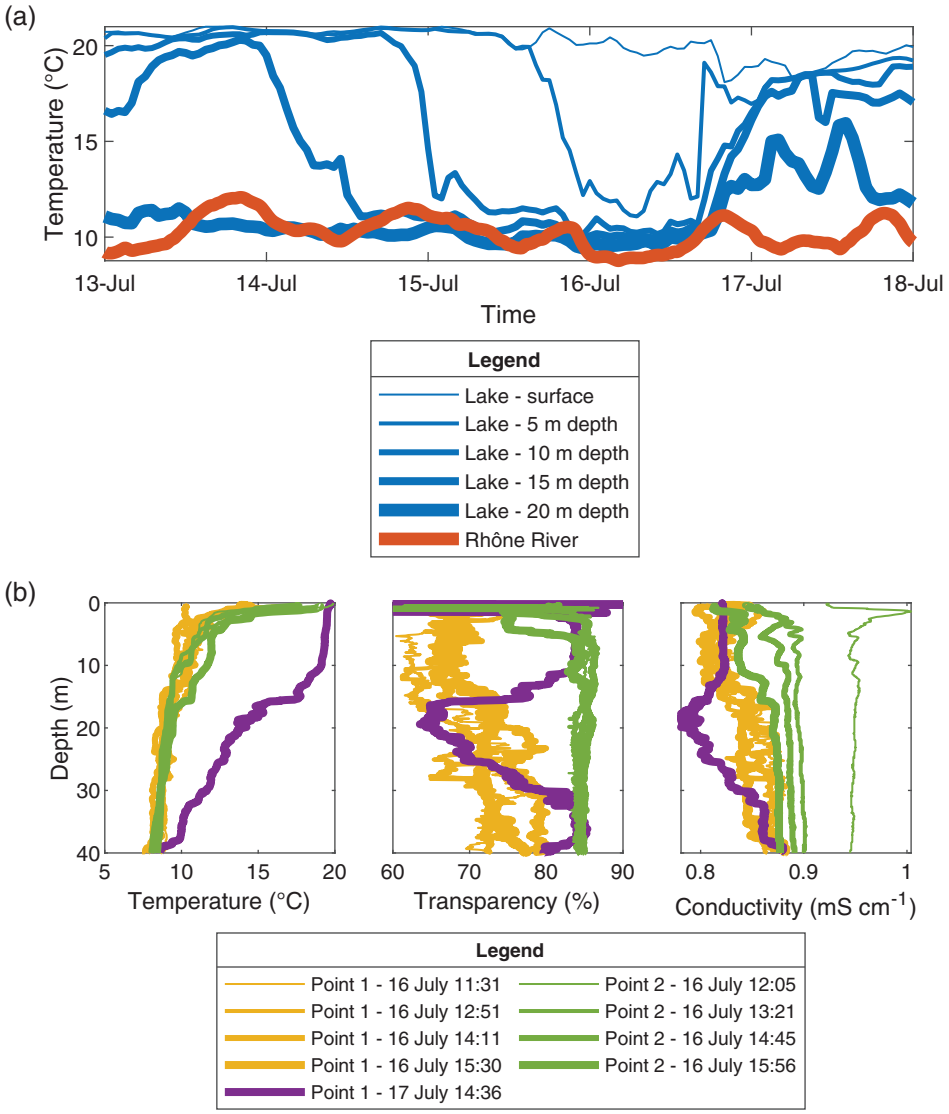

Fig. 4. (**a**) Time series of simulated water temperature in the lake in front of the river inflow (mean of points 2 and 3) at five different depths, and observed Rhône River temperature. (**b**) Vertical profiles of water temperature (left panel), transparency (center) and conductivity (right panel) for Episode 2 measured at points 1 and 2. Colors and lines are detailed in the legend. *See* Fig. 1b for locations.

et al. 2005). Thus, with each passage of the upwelling end of the Kelvin wave in the Bouveret area, a deviation of the river plume, as described for Episode 2, can reoccur. However, generally, the amplitude of a consecutive passage is smaller due to energy loss caused by bottom friction; thus, the effect will be less noticeable. The intensity of this deviation also depends on the Rhône River discharge dynamics.

The structure of currents related to coastal upwelling in the Rhône delta area is documented by the field measurements taken in the nearshore region (Fig. 9a). The limited offshore extent of these currents and their depth profile were obtained from the 3D numerical modeling (Fig. 6). This current pattern resembles that of a shore-hugging Kelvin wave where strong currents are limited to the nearshore area and rapidly taper off with distance from shore (Mortimer 2004). The coastal upwelling in Episode 2 passes counterclockwise from the southern shore to the northern shore of the lake in about 36 h (Fig. 3). This is slightly less than one half of a Kelvin wave period during summer stratification (Lemmin et al. 2005). Thus, the coastal upwelling observed in this study presents Kelvin wave-like features as was reported by Beletsky et al. (1997).

These results confirm that the high-magnitude currents measured at Points 2 and 3 (Fig. 5) and the deviation of the river plume seen in the surface images taken by the time-lapse cameras (Figs. 7 and 8) are caused by a jet-like alongshore current confined to the nearshore zone in a near surface layer of limited depth. After stratification is re-established (Fig. 4) on 17 July 2019, the plume surface pattern disappears in the images (Figs. 7 and 8), indicating a plume interflow (Fig. 9). At

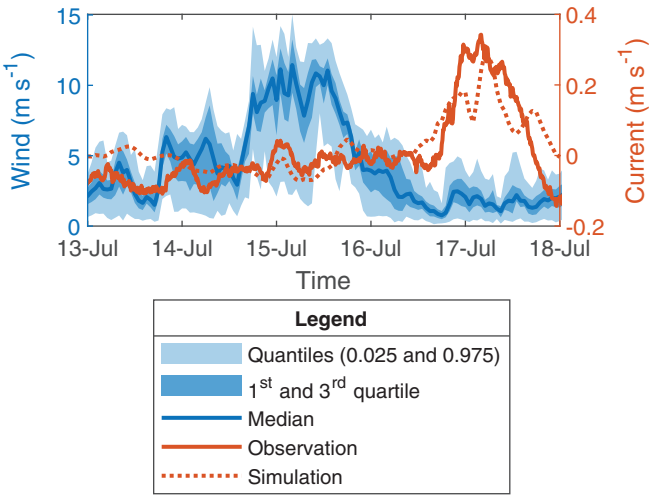

Fig. 5. Time series of wind speed over the lake (COSMO data, left *y*-axis, blue), and predicted and measured eastward current velocity at Bouveret (mean of points 2 and 3, and averaged between 5 and 15-m depth, right *y*-axis, red) for episode 2. Colors and lines are detailed in the legend.

the same time, alongshore eastward currents measured in the ADCP transect remain high in the near surface zone (Fig. 9) and agree with the model current patterns in the Bouveret area (Fig. 6). It can therefore be expected that the interflow will continue to be deviated to the east for some time. During the passage of the coastal upwelling in the Rhône River delta area, the minima in the temperature pattern and maxima in the velocity pattern in the coastal upwelling do not coincide. When alongshore currents in the upper layers were highest early on 17 July, stratification was weak and, as a result, gradient Richardson numbers in these layers were low, indicating a strong potential for mixing.

Rhône River plume

As indicated in the Materials and methods section, the Rhône River water density is on average always higher than that of the lake during the stratification period. The normally expected behavior of river intrusions for this situation is that the river inflow pushes the lake surface water to a plunge point where the river intrusion abruptly sinks, and follows the lakebed as an underflow. Then, due to interactions with the vertical lake density profile, the river intrusion detaches from the lakebed at the depth where river inflow and lake densities are comparable and subsequently moves as an interflow, most often in the thermocline layer. In the plunge region, vigorous entrainment of ambient lake water into the unconfined river inflow occurs, reducing the excess density of the entering river waters.

Most RGB and thermal images taken during summer stratification by the time-lapse cameras installed above the Bouveret area confirm that the river water plunges shortly after the inflow, with the plunge line describing a quasi-isosceles triangle, whose base coincides with the river mouth (*see* Fig. S15 for RGB and thermal images for this river inflow configuration). This suggests that, during the stratification period, the Rhône River plume mainly flows as an interflow in the thermocline layer as indicated by previous measurements (Giovanoli and Lambert 1985). The interflow is carried offshore and its subsequent displacement in the lake is determined by large-scale circulation. It was shown that the interflow follows pathways guided by large-scale gyres (Razmi et al. 2018; Cimatoribus et al. 2019) that further offshore can deviate the plume and transport it to the northern shore. Thereafter, it moves along the northern shore and either it reaches the outflow in Geneva within a few days or it gets trapped for lengthy periods in the major gyres in the central part of the lake (Cimatoribus et al. 2019).

Our detailed investigation of Episode 2 makes evident that, during the passage of a coastal upwelling event, two important differences from the standard, large-scale interflow concept for negatively buoyant rivers occur:

- The Rhône River does not plunge, indicating that the densities of the river and of the near surface layer of the lake are comparable. Since the Rhône River discharge and temperature varied little during that time (Table ST1), the observed change in the plume dynamics can only be caused by processes occurring in the lake. This was confirmed by the observed sequence of processes (summarized in Fig. 10), resulting in a rapid and drastic change in lake stratification during the passage of the coastal upwelling. As documented by repeated CTD profiles and ADCP transects (Figs. 4b and 9), this led to an almost homogeneous temperature over the whole water column, which is colder than the epilimnion temperature at this time of the year. In this situation, river and lake densities were comparable, and thus, the river inflow was distributed throughout the water column near the Rhône River mouth. This dramatically affects the mixing and entrainment of the river plume.
- In contrast to the large-scale interflow pattern, during the passage of the cold coastal upwelling, the Rhône River plume is deviated to the east in the nearfield of the inflow (Figs. 7 and 8) by strong alongshore currents in the nearshore zone. This causes the plume to flow along the eastern shore in the nearshore zone, where the lake is shallow. Thus, during this deviation, river sediments (coarse and fine) are transported over this shallow zone and are deposited there, instead of being advected into the deeper areas. In previous work, dynamic penetrometer measurements carried out in this nearshore zone to the east of the Rhône River mouth found a thick layer of loose fine sediments of Rhône River origin, at times containing a high concentration of decomposing organic matter (Nina Stark, pers. comm.; Stark et al. 2013). This suggests that deposition of this sediment is a recurring process that can be explained by our observations during Episode 2.

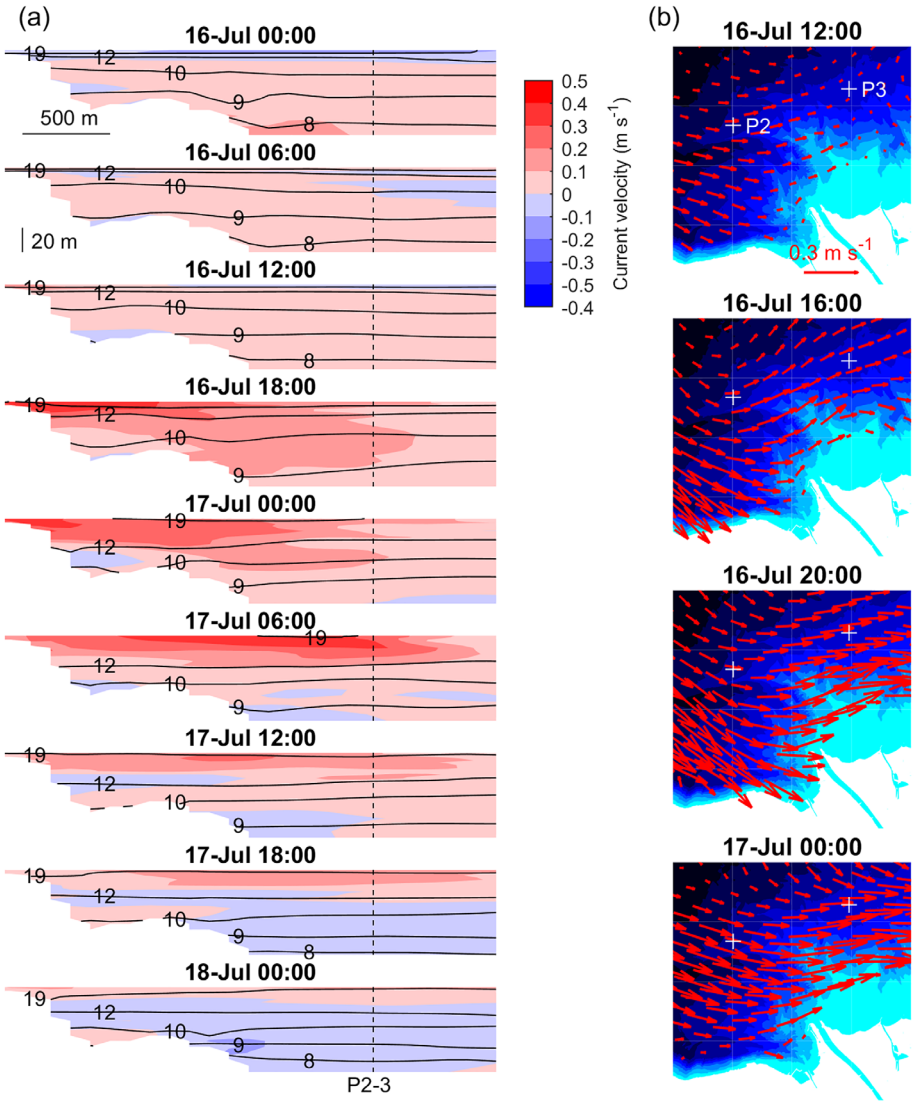

Fig. 6. Episode 2: (**a**) Filled contour plots of simulated current velocity perpendicular to the plane of the section (*see* Fig. 1b) across Lake Geneva, close to the axis of the Rhône River inflow. The velocity range is given in the color bar; positive values are "exiting" the page, that is, moving eastwards. Isotherms (8°C, 9°C, 10°C, 12°C, and 19°C) are also shown. The Rhône River inflow is on the left side of each panel. The vertical dashed line indicates the intersection of the line connecting points 2 and 3 with the section. (**b**) Quiver plots of simulated current velocity at the Bouveret area. Current velocity is averaged between 5 and 15 m depth. In the area east of the Rhône River inflow, no current velocity can be given because of the shallow depths (<5 m). The two white crosses indicate the location of points 2 and 3. *See* Fig. 1b for location of the section and the Bouveret area.

Comparing the current pattern (Fig. 9a) and the backscattering pattern (Fig. 9b) of the sequence of ADCP transects taken during the 2 days of Episode 2, some interesting features can be observed:

- The backscattering always spreads over a wider area than the velocity, indicating that strong lateral mixing occurs between the Rhône River plume and the ambient lake waters due to entrainment.
- The strong eastward currents in the epilimnion on 17 July at 10:36 and 11:32 push the sediments of the river plume to the east where water depth rapidly decreases, moving the particle cloud up to the surface in that area (Fig. 7; 17 July at 9:00). This shows the effect of bottom topography in guiding the plume and is consistent with the penetrometer measurements discussed above.
- Even when the plume forms an interflow, sediment particles are distributed in the hypolimnion below the interflow down to the lake bottom. This indicates that particles are continuously settling out below the interflow. In our previous measurements (not shown here), particle sizes up to 60 μm were found in the interflow and in the hypolimnion below it.
- When strong westward currents occurred in the thermocline layer on 17 July 2019 at 13:28, particles from the interflow were also spread out to the west of the center of

Fig. 7. Episode 2: Hourly RGB images taken by the RGB time lapse camera covering the period of current velocity measurements presented in Fig. 5. The Rhône River water entering Lake Geneva from the channel at the bottom of the images is light brown due to high suspended load. The river channel is about 120-m wide. Compare with thermal images in Fig. 8, in particular the deviation of the Rhône inflow on 16 July at 18:00. *See* Fig. 1b for the camera viewing angle. The circular line is a floating barrier used to retain driftwood.

the interflow. Over time, the accumulation of particles below the interflow and to the west of it builds up a layer of loose unconsolidated particles at the entrance of the Rhône River canyon with slope over-steepening that affects slope stability. It was hypothesized that these sediments contribute to the development of gravitational processes such as turbidity currents in the canyon (Corella et al. 2014).

- Occasionally, isolated features of strong backscattering are seen outside the plume pattern (Fig. 9b). These may indicate coherent structures shedding from the plume due to large-scale entrainment. Such large-scale structures were visible when the river plume reached the surface during the passage of the coastal upwelling in the early image on 16 July (Figs. 7 and 8). In the RGB and thermal images taken during the summer, patches of the turbid and cold river water are often visible beyond the plunge line in the interflow region and rapidly disappear. The patches can be interpreted as "boils" rising from the river plume to the surface, due to large-scale instabilities at the interface between the plume and the ambient water. The boils observed on the surface and the strong backscattering features (Fig. 9b) may document the same phenomenon.

The passage of a cold coastal upwelling, therefore, strongly affects the transport and deposition dynamics of sediments, brought into the lake by the Rhône River, in the river delta and the adjacent near shore area for the range of river discharge being investigated here.

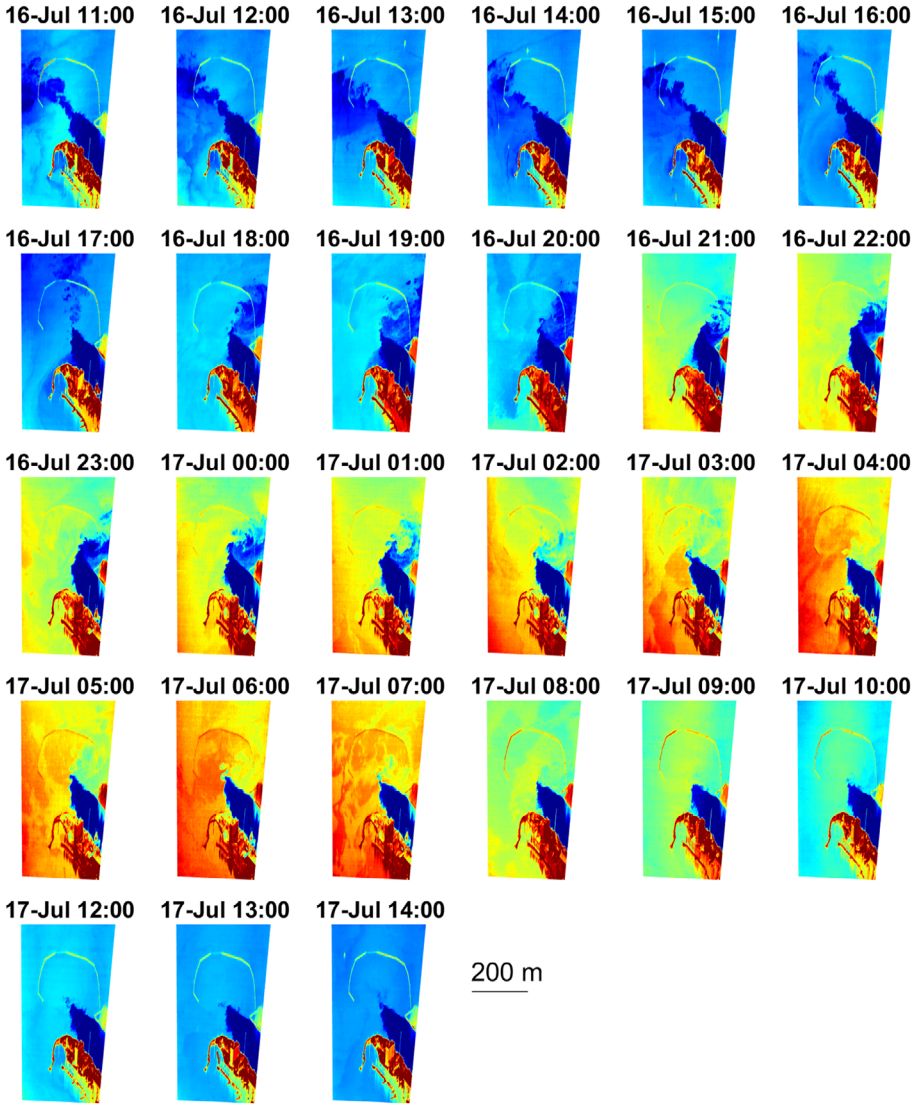

Fig. 8. Episode 2: Hourly thermal images taken by the infrared time-lapse camera covering the time period of the current velocity measurements presented in Fig. 5. Dark blue pixels in the Rhône River plume correspond to cold river temperatures of approximately 10°C (Fig. 4). During the night (16 July at 21:00 to 17 July at 9:00), images are perturbed by a humid atmospheric boundary layer generated by evaporation. Compared with RGB images in Fig. 7. *See* Fig. 1b for the camera viewing angle. The circular line is a floating barrier used to retain driftwood.

This transport dynamics may have an effect of the biogeochemical balance in the Rhône River inflow area. A significant decrease of nutrient concentration within the surface mixed layer was reported during the stratification period at the SHL2 station in the center of the lake (CIPEL 2019). However, in the eastern part of Lake Geneva, where the Rhône River enters the lake, a phytoplankton bloom near the lake surface is observed (Kiefer et al. 2015; Bouffard et al. 2018; Soulignac et al. 2018). The change in Rhône River plume dynamics due to the passage of the cold coastal upwelling presented in this study suggests that it could contribute to feeding the lake surface layer with nutrients by horizontal mixing in the euphotic layer. This is supported by low, model-based gradient Richardson numbers found during the passage of the coastal upwelling (Fig. S16). Strong shear in a near surface layer and a relatively weak stratification provide for considerable turbulent mixing between these two different water masses, and water and particles transported by the Rhône River plume, which are known to carry nutrients, will be kept in suspension near the phototrophic zone. It was observed that counterclockwise progressing coastal upwelling occurred another four times during the summer of 2019 (*see* Appendix S1). Coastal upwelling can, therefore, be considered a frequently recurrent phenomenon during the stratification period, and the cumulative effect in time of this transient process in the near shore area may be significant, at least in the near field of the Rhône River inflow.

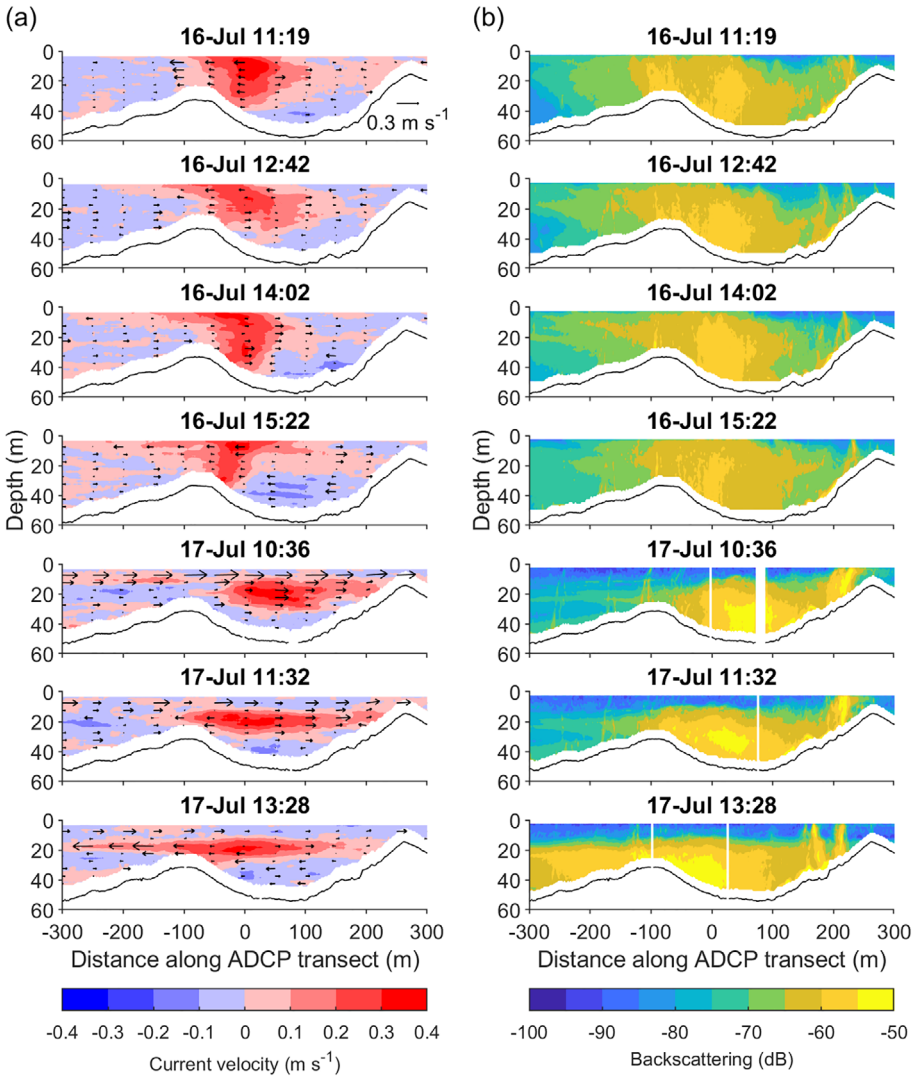

Fig. 9. Episode 2: (**a**) Filled contour plots of measured (ADCP) current velocity perpendicular to the plane of the ADCP transect (Fig. 1b) and quiver plots of the transversal component; positive values are "entering" the page, i.e., moving out into the lake. (**b**) Filled contour plots of the observed ADCP backscattering intensity in the ADCP transect. The black line represents the lake bottom contour. Near bottom current velocities are omitted. Current velocity and backscattering ranges are given in the legends.

Summary and conclusions

Investigations carried out in Lake Geneva during summer stratification in 2019 allowed documenting the rapid change of river interflow dynamics caused by the passage of a coastal upwelling event. For the first time, the interaction of negatively buoyant river inflow and transient coastal upwelling in a large lake was observed, and with such detail, by analyzing in situ measurements, lake surface imagery, and high-resolution numerical modeling results. It was shown that this rapid change is the result of the following sequence of processes (summarized in Fig. 10) that were initiated in one part of the lake and then passed through the Rhône River mouth area:

- Coastal upwelling generated on the southern shore by a strong *Bise* wind, blowing long enough, (i.e., with the duration exceeding the lake's inertial period), progresses Kelvin wave-like counterclockwise around the lake basin in the nearshore zone after the wind has ceased.
- When it reaches the area of the Rhône River inflow, the upwelling homogenizes the lake temperature in the nearshore zone, resulting in a well-mixed (compared with its stratified state) profile with a density close to that of the Rhône River.
- This, in turn, abruptly transforms the Rhône River plume from an interflow into an intrusion that spreads over the whole water column.

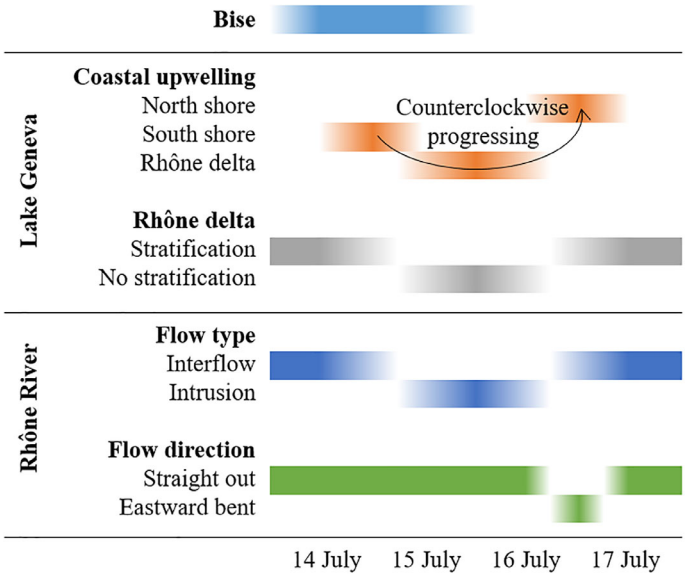

Fig. 10. Episode 2: Schematic representation summarizing the sequence of processes, initiated by a *Bise* wind event, that took place in the lake during the passage of the counterclockwise progressing cold coastal upwelling in the Bouveret area. This resulted in a strong change in Rhône River dynamics.

- Concurrently, the river plume is sharply deviated by the strong alongshore currents resulting from the passage of the upwelling such that it no longer flows out along the axis of the river, but perpendicular to it, that is, along the shore in the nearshore region.
- During this period, the river plume can bring nutrients directly into the phototrophic near-surface layer and may locally create a hotspot of phytoplankton development. The upwelling affects an area of more than 1 km offshore and several km alongshore.
- After the passage of the coastal upwelling, thermal stratification is re-established, and the negatively buoyant Rhône River inflow again plunges and transforms into an interflow in the thermocline layer, and moves straight out into the lake in the axis of the river.
- The above sequence of events occurs frequently during the stratified period, suggesting that their cumulative effects will be significant (e.g., on sediment transport and nutrient availability).

These observations provided details of the sequence of processes involved for one episode (Episode 2). However, a comparable river plume displacement and deviation also occurred during the remaining four episodes from 24 June to 15 September 2019. The moored ADCP data, surface images, and numerical modeling results confirm that the same sequence of processes took place in all five episodes. Previously, it was shown that *Bise* winds with wind speeds >3 m s^{-1} occur about 23% of the time during the stratification period (Razmi et al. 2018). Coastal upwelling and its effect on the Rhône River inflow can, therefore, be considered a recurrent phenomenon during the stratification period that has a significant impact on the spreading of the river plume, and potentially, on lake ecosystem dynamics.

Based on the detailed documentation and the frequency of these episodes, the longstanding concept that stable interflows centered in the thermocline layers are a quasi-steady state feature for negatively buoyant rivers throughout the stratified period should be revised. As the present study demonstrated, highly nonstationary transient processes, such as the passage of coastal upwelling, can temporarily, yet significantly, alter the nearshore dynamics of a river inflow. These transient processes were shown to occur frequently during the stratification period. Since counterclockwise progressing coastal upwelling has also been reported in other large lakes, this sequence of processes observed in Lake Geneva can be expected to occur in other large lakes with comparable wind-induced large-scale thermocline displacements.

Note that 3D concepts are needed to explain these frequent, episodic observations. Furthermore, it was demonstrated that a combination of field measurements with moored instruments, complemented by detailed in situ campaigns, remote sensing, 3D numerical modeling, and well-documented background data provide an ideal tool set to advance the understanding of such complex and thus far undocumented processes that are likely important for lake ecosystem dynamics. The consistency (both temporally and spatially) between the field observations and the high-resolution numerical modeling results observed here provides confidence that high-resolution 3D numerical modeling using a calibrated model is a suitable and reliable tool for studying details of rapidly changing physical processes in lakes, thus greatly extending the interpretation of point-wise field measurements.

References

Alavian, V., G. H. Jirka, R. A. Denton, M. C. Johnson, and H. G. Stefan. 1992. Density currents entering lakes and reservoirs. J. Hydraul. Eng. ASCE **118**: 1464–1489. doi:10.1061/(ASCE)0733-9429(1992)118:11(1464)

Allan, R. J., A. Mudroch, and A. Sudar. 1983. An introduction to the Niagara River/Lake Ontario pollution problem. J. Great Lakes Res. **9**: 111–117. doi:10.1016/S0380-1330(83)71881-2

Bauer, S. W., W. H. Graf, C. H. Mortimer, and C. Perrinjaquet. 1981. Inertial motion in Lake Geneva (Le Léman). Arch. Meteorol. Geophys. Bioclimatol. A **30**: 289–312. doi:10.1007/bf02257850

Beletsky, D., W. P. O'Connor, D. J. Schwab, and D. E. Dietrich. 1997. Numerical simulation of internal kelvin waves and coastal upwelling fronts. J. Phys. Oceanogr. **27**: 1197–1215 doi:10.1175/1520-0485(1997)027<1197:NSOIKW>2.0.CO;2.

Bolgrien, D. W, and A. S Brooks. 1992. Analysis of thermal features of lake michigan from AVHRR satellite images. J. Great Lakes Res. **18**: 259–266. doi:10.1016/S0380-1330(92)71293-3

Bouffard, D., I. Kiefer, A. Wüest, S. Wunderle, and D. Odermatt. 2018. Are surface temperature and chlorophyll in a large deep lake related? An analysis based on satellite observations in synergy with hydrodynamic modelling and in-situ data. Remote Sens. Environ. **209**: 510–523. doi:10.1016/j.rse.2018.02.056

Churchill, J. H., E. A. Ralph, A. M. Cates, J. W. Budd, and N. R. Urban. 2003. Observation of a negatively buoyant river plume in a large lake. Limnol. Oceanogr. **48**: 884–894. doi:10.4319/lo.2003.48.2.0884

Cimatoribus, A. A., U. Lemmin, D. Bouffard, and D. A. Barry. 2018. Nonlinear dynamics of the nearshore boundary layer of a large lake (Lake Geneva). J. Geophys. Res. Oceans **123**: 1016–1031. doi:10.1002/2017JC013531

Cimatoribus, A. A., U. Lemmin, and D. A. Barry. 2019. Tracking Lagrangian transport in Lake Geneva: A 3D numerical modeling investigation. Limnol. Oceanogr. **64**: 1252–1269. doi:10.1002/lno.11111

CIPEL, 2019. Rapports sur les études et recherches entreprises dans le bassin lémanique, Campagne 2018, Commission internationale pour la protection des eaux du Léman (CIPEL), Nyon. Available from https://www.cipel.org/wp-content/uploads/2019/10/RapportScientifique_camp_2018-1.pdf, .

Corella, J. P., A. Arantegui, J.-L. Loizeau, T. DelSontro, N. le Dantec, N. Stark, F. S. Anselmetti, and S. Girardclos. 2014. Sediment dynamics in the subaquatic channel of the Rhone delta (Lake Geneva, France/Switzerland). Aquat. Sci. **76**: 73–87. doi:10.1007/s00027-013-0309-4

Corella, J. P., J.-L. Loizeau, K. Kremer, M. Hilbe, J. Gerard, N. le Dantec, N. Stark, M. Gonzalez-Quijano, and S. Girardclos. 2016. The role of mass-transport deposits and turbidites in shaping modern lacustrine Deepwater channels. Marine Petrol. Geol. **77**: 515–525. doi:10.1016/j.marpetgeo.2016.07.004

Csanady, G. T. 1977. Intermittent "full" upwelling in Lake Ontario. J. Geophys. Res. **82**: 397–419. doi:10.1029/JC082i003p00397

Demchenko, N., C. He, Y. R. Rao, and R. Valipour. 2017. Surface river plume in a large lake under wind forcing: Observations and laboratory experiments. J. Hydrol. **553**: 1–12. doi:10.1016/j.jhydrol.2017.07.025

Dominik, J., D. Burrus, and J. P. Vernet. 1983. A preliminary investigation of the Rhone River plume in eastern Lake Geneva. J. Sediment. Petrol. **53**: 159–163. doi:10.1306/212F817A-2B24-11D7-8648000102C1865D

Dorostkar, A., L. Boegman, and A. Pollard. 2017. Three-dimensional simulation of high-frequency nonlinear internal wave dynamics in Cayuga Lake. J. Geophys. Res. Oceans **122**: 2183–2204. doi:10.1002/2016JC011862

Gan, J., L. Li, D. Wang, and X. Guo. 2009. Interaction of a river plume with coastal upwelling in the northeastern South China Sea March. Cont. Shelf Res. **29**: 728–740. doi:10.1016/j.csr.2008.12.002

Garvine, R. W. 1995. A dynamical system for classifying buoyant coastal discharges. Continent. Shelf Res. **15**: 1585–1596. doi:10.1016/0278-4343(94)00065-U

Giovanoli, F., and A. Lambert. 1985. Die Einschichtung der Rhone im Genfersee: Ergebnisse von Strömungsmessungen im August 1983. Swiss J. Hydrol. **47**: 159–178. doi:10.1007/BF02551939

Giovanoli, F. 1990. Horizontal transport and sedimentation by interflows and turbidity currents in Lake Geneva, p. 175–195. *In* M. M. Tilzer and C. Serruya [eds.], Large Lakes. Brock/Springer Series in Contemporary Bioscience. Berlin, Heidelberg: Springer. doi:10.1007/978-3-642-84077-7_9

Graf, W. H., and J. P. Prost. 1980. Aerodynamic drag and its relation to the sea state: With data from Lake Geneva. Archiv für Meteorologie, Geophysik und Bioklimatologie Serie A **29**: 67–87. doi:10.1007/BF02247734

Griffies, S. M., and R. W. Hallberg. 2000. Biharmonic friction with a Smagorinsky-like viscosity for use in large-scale eddy-permitting ocean models. Mon. Weather Rev. **128**: 2935–2946 doi:10.1175/1520-0493(2000)128<2935:BFWASL>2.0.CO;2.

Hogg, C. A. R., C. L. Marti, H. E. Huppert, and J. Imberger. 2013. Mixing of an interflow into the ambient water of Lake Iseo. Limnol. Oceanogr. **58**: 579–592. doi:10.4319/lo.2013.58.2.0579

Jirka, G. H. 2007. Buoyant surface discharges into water bodies. II: Jet integral model. J. Hydraul. Eng.-ASCE **133**: 1021–1036. doi:10.1061/(ASCE)0733-9429(2007)133:9(1021)

Kiefer, I., D. Odermatt, O. Anneville, A. Wüest, and D. Bouffard. 2015. Application of remote sensing for the optimization of in-situ sampling for monitoring of phytoplankton abundance in a large lake. Sci. Total Environ. **527**: 493–506. doi:10.1016/j.scitotenv.2015.05.011

Krauss, W. 1973. Dynamics of the homogeneous and quasi-homogeneous ocean, v. **1**. Berlin: Gebrüder Borntraeger.

Kremer, K., J. P. Corella, M. Hilbe, F. Marillier, D. Dupuy, G. Zenhausern, and S. Girardclos. 2015. Changes in distal sedimentation regime of the Rhone delta system controlled by subaquatic channels (Lake Geneva, Switzerland/France). Mar. Geol. **370**: 125–135. doi:10.1016/j.margeo.2015.10.013

Large, W. G., J. C. McWilliams, and S. C. Doney. 1994. Oceanic vertical mixing: A review and a model with a nonlocal boundary layer parameterization. Rev. Geophys. **32**: 363–403. doi:10.1029/94RG01872

Large, W. G., and S. Pond. 1981. Open Ocean momentum flux measurements in moderate to strong winds. J. Phys. Oceanogr. **11**: 324–336 doi:10.1175/1520-0485(1981)011<0324:OOMFMI>2.0.CO;2.

Laval, B. E., J. Morrison, D. J. Potts, E. C. Carmack, S. Vagle, C. James, F. A. McLaughlin, and M. Foreman. 2008. Wind-driven summertime upwelling in a Fjord-type lake and its impact on downstream river conditions: Quesnel Lake and River, British Columbia, Canada. J. Great Lakes Res. **34**: 189–203 doi:10.3394/0380-1330(2008)34[189:WSUIAF]2.0.CO;2.

Lemmin, U. 2020. Insights into the dynamics of the deep hypolimnion of Lake Geneva as revealed by long-term temperature, oxygen, and current measurements. Limnol. Oceanogr. **65**: 2092–2107. doi:10.1002/lno.11441

Lemmin, U., and N. D'Adamo. 1996. Summertime winds and direct cyclonic circulation: Observations from Lake Geneva. Ann. Geophys. **14**: 1207–1220. doi:10.1007/s00585-996-1207-z

Lemmin, U., C. H. Mortimer, and E. Bauerle. 2005. Internal seiche dynamics in Lake Geneva. Limnol. Oceanogr. **50**: 207–216. doi:10.4319/lo.2005.50.1.0207

Lisi, P. J., and D. E. Schindler. 2015. Wind-driven upwelling in lakes destabilizes thermal regimes of downstream rivers. Limnol. Oceanogr. **60**: 169–180. doi:10.1002/lno.10010

Loizeau, J.-L., and J. Dominik. 2000. Evolution of the Upper Rhone River discharge and suspended sediment load during the last 80 years and some implications for Lake Geneva. Aquat. Sci. **62**: 54–67. doi:10.1007/s000270050075

Marshall, J., A. Adcroft, C. Hill, L. Perelman, and C. Heisey. 1997. A finite-volume, incompressible Navier Stokes model for studies of the ocean on parallel computers. J. Geophys. Res. Oceans **102**: 5753–5766. doi:10.1029/96JC02775

Masse, A. K., and C. R. Murthy. 1990. Observations of the Niagara River thermal plume (Lake Ontario, North America). J. Geophys. Res. Oceans **95**: 16097–16109. doi:10.1029/JC095iC09p16097

Monsen, N. E., J. E. Cloern, L. V. Lucas, and S. G. Monismith. 2002. A comment on the use of flushing time, residence time, and age as transport time scales. Limnol. Oceanogr. **47**: 1545–1553. doi:10.4319/lo.2002.47.5.1545

Mortimer, C. H. 2004. Lake Michigan in motion: Responses of an inland sea to weather, earth-spin and human activities. Milwaukee: Univ. of Wisconsin Press.

Mortimer, C. H. 1988. Discoveries and testable hypotheses arising from coastal zone color scanner imagery of southern Lake Michigan. Limnol. Oceanogr. **33**: 203–226. doi:10.4319/lo.1988.33.2.0203

Mortimer, C. H. 1974. Lake hydrodynamics. Internationale Vereinigung für Theoretische und Angewandte Limnologie: Mitteilungen **20**: 124–197. doi:10.1080/05384680.1974.11923886

Oesch, D., J. M. Jaquet, R. Klaus, and P. Schenker. 2008. Multi-scale thermal pattern monitoring of a large lake (Lake Geneva) using a multi-sensor approach. Int. J. Remote Sens. **29**: 5785–5808. doi:10.1080/01431160802132786

Osadchiev, A., K. Silvestrova, and S. Myslenkov. 2020. Wind-driven coastal upwelling near large river deltas in the Laptev and east-Siberian seas. Remote Sens. (Basel) **12**: 844. doi:10.3390/rs12050844

Plattner, S., D. M. Mason, G. A. Leshkevich, D. J. Schwab, and E. S. Rutherford. 2006. Classifying and forecasting coastal upwellings in Lake Michigan using satellite derived temperature images and buoy data. J. Great Lakes Res. **32**: 63–76 doi:10.3394/0380-1330(2006)32[63:CAFCUI]2.0.CO;2.

Rahaghi, A. I., U. Lemmin, A. Cimatoribus, D. Bouffard, M. Riffler, S. Wunderle, and D. A. Barry. 2018. Improving surface heat flux estimation for a large lake through model optimization and two-point calibration: The case of Lake Geneva. Limnol. Oceanog. Meth. **16**: 576–593. doi:10.1002/lom3.10267

Razmi, A. M., D. A. Barry, D. Bouffard, T. Vennemann, C. E. Barry, and U. Lemmin. 2018. Currents of Lake Geneva, p. 141–172. *In* N. Chèvre [ed.], Micropollutants in large lakes: From potential pollution to risk assessments. Lausanne: EPFL Press. doi:10.1201/9781351240291

Reiss, R. S., U. Lemmin, A. A. Cimatoribus, and D. A. Barry. 2020. Wintertime coastal upwelling in Lake Geneva: An efficient transport process for deepwater renewal in a large, deep lake. J. Geophys. Res.-Oceans **125**: e2020JC016095. doi:10.1029/2020JC016095

Rimet, F., and others. 2020. The Observatory on LAkes (OLA) database: Sixty years of environmental data accessible to the public. J. Limnol. **79**: 164–178. doi:10.4081/jlimnol.2020.1944

Scheu, K. R., D. A. Fong, S. G. Monismith, and O. B. Fringer. 2015. Sediment transport dynamics near a river inflow in a large alpine lake. Limnol. Oceanogr. **60**: 1195–1211. doi:10.1002/lno.10089

Shinohara, R., T. Okunishi, K. Adachi, L. S. Viet, H. Mine, T. Yamashita, and M. Isobe. 2008. Evaluation of the impact of water dilution within the hypereutrophic Lake Barato, Japan. Lake Reservoir Manag **24**: 301–312. doi:10.1080/07438140809354840

Simons, T. J., and W. M. Schertzer. 1987. Stratification, currents, and upwelling in lake ontario, summer 1982. Can. J. Fish. Aquat. Sci. **44**. doi:10.1139/f87254

Soulignac, F., and others. 2018. Using 3D modeling and remote sensing capabilities for a better understanding of spatio-temporal heterogeneities of phytoplankton abundance in large lakes. J. Great Lakes Res. **44**: 756–764. doi:10.1016/j.jglr.2018.05.008

Stark, N., N. Le Dantec, J. P. Corella, D. A. Barry, U. Lemmin, S. Girardclos, and A. Kopf. 2013. Deployment of a dynamic penetrometer from manned submersibles for fine-scale geomorphology studies. Limnol. Oceanogr. Meth. **11**: 529–539. doi:10.4319/lom.2013.11.529

Valipour, R., L. F. Léon, D. Depew, A. Dove, and Y. R. Rao. 2016. High-resolution modeling for development of nearshore ecosystem objectives in eastern Lake Erie. J. Great Lakes Res. **42**: 1241–1251. doi:10.1016/j.jglr.2016.08.011

Voudouri, A., E. Avgoustoglou, and P. Kaufmann. 2017. Impacts of observational data assimilation on operational forecasts, p. 143–149. *In* T. Karacostas, A. Bais, and P. T. Nastos [eds.], Perspectives on atmospheric sciences. Lausanne: Springer International Publishing. doi:10.1007/978-3-319-35095-0_21

Wanner, H., and M. Furger. 1990. The Bise-climatology of a regional wind north of the Alps. Meteorol. Atmos. Phys. **43**: 105–115. doi:10.1007/BF01028113

Welch, E. B. 1981. The dilution-flushing technique in lake restoration. Water Resour. Bull. **17**: 558–564. doi:10.1111/j.1752-1688.1981.tb01260.x

Zhao, H. X., X. J. Duan, B. Stewart, B. S. You, and X. W. Jiang. 2013. Spatial correlations between urbanization and river water pollution in the heavily polluted area of Taihu Lake Basin, China. J. Geogr. Sci. **23**: 735–752. doi:10.1007/s11442-013-1041-7

Acknowledgments

The authors acknowledge support from the Swiss National Science Foundation (SNSF) under grants 159422 and 178866. The authors thank Koen Blanckaert and Rob Uittenbogaard for fruitful discussions at the early stage of this study, as well as SAGRAVE (http://www.sagrave.ch/) for their assistance with logistics.

Conflict of interest

The authors declare no conflicts of interest.

Submitted 13 July 2020
Revised 23 November 2020
Accepted 22 May 2021

Associate editor: Werner Eckert